Gouy Phase Radial Mode Sorter for Light: Concepts and Experiments

Xuemei Gu,[1,2,*] Mario Krenn,[1,3,†] Manuel Erhard,[1,3] and Anton Zeilinger[1,3,‡]

[1]*Institute for Quantum Optics and Quantum Information (IQOQI), Austrian Academy of Sciences,
Boltzmanngasse 3, 1090 Vienna, Austria*

[2]*State Key Laboratory for Novel Software Technology, Nanjing University,
163 Xianlin Avenue, Qixia District, 210023 Nanjing City, China*

[3]*Vienna Center for Quantum Science & Technology (VCQ), Faculty of Physics, University of Vienna,
Boltzmanngasse 5, 1090 Vienna, Austria*

We present an in principle lossless sorter for radial modes of light, using accumulated Gouy phases. The experimental setups have been found by a computer algorithm, and can be intuitively understood in a geometric way. Together with the ability to sort angular-momentum modes, we now have access to the complete two-dimensional transverse plane of light. The device can readily be used in multiplexing classical information. On a quantum level, it is an analog of the Stern-Gerlach experiment—significant for the discussion of fundamental concepts in quantum physics. As such, it can be applied in high-dimensional and multiphotonic quantum experiments.

Introduction.—The spatial modes of light give access to an in principle unbounded state space. This allows us to encode information in higher-dimensional alphabets beyond one bit per photon. A particularly well-studied mode family are the Laguerre-Gaussian (LG) modes [1]. One of the special features of LG modes is that they carry well-defined $\ell\hbar$ quanta of orbital-angular momentum (OAM) where ℓ is one of the two numbers that define the LG modes [2]. Over the last 25 years, a large toolbox has been developed to generate [3–5] and manipulate [6–11] OAM modes. This has led to a manifold of applications ranging from classical high-speed [12,13] and long-distance [14,15] communication to high-dimensional quantum entanglement [16–19] and quantum cryptography [20–22].

The second much less investigated degree of freedom of the LG modes is the radial quantum number p [23–25]. It spans a second completely independent and in principle unbounded state space, with the same capability to encode a vast amount of information. Its quantum character has been demonstrated by two-photon interference [26] and quantum correlations and entanglement between radial modes have been demonstrated [27,28]. The only real manipulation of radial modes known so far has been demonstrated using the potential of controlled random material, in order to sort different radial modes [29]. Unfortunately the manipulation works in a lossy way which made its application in classical and quantum experiments challenging so far. In order to exploit the full potential of the radial modes, the available toolbox needs to be expanded.

Here we show how higher-order spatial modes of light—in particular their radial modes—can be sorted with theoretically 100% visibility. For that, we use an interferometer with a mode-dependent phase difference. This concept has been used for other degrees of freedom (such as a mode sorter for OAM modes in Ref. [6], or in a theoretical proposal for a more general interferometric sorting scheme [30]). The challenging question then is: How can one experimentally achieve mode dependent phase shifters for radial modes? We answer this question with the help of a computer algorithm [31]: One of the two arms in the interferometer contains a lens configuration, which leads to a difference in the accumulated Gouy phase $\Delta\varphi_g$. We show experimentally a phase difference of $\Delta\varphi_g = (\pi/2)$ and $\Delta\varphi_g = (\pi/4)$, and apply it to sort different spatial modes. We also theoretically demonstrate phase differences of $\Delta\varphi_g = (\pi/n)$ ($2 \leq n \leq 8$).

Our technique can readily be applied to classical experiments [such as (de)multiplexing in classical communication] or quantum experiments (such as two-photon interference for high-dimensional entanglement). Our intuitive geometric interpretation of the technique can be used to unify and generalize several similar approaches.

Spatial modes and the Gouy phase.—The paraxial wave equation in cylindric coordinates leads to Laguerre-Gaussian mode solutions, which are denoted as

$$\mathrm{LG}_{p,\ell}(r,\phi,z)$$
$$= \sqrt{\frac{2p!}{\pi(p+|\ell|)!}}\frac{1}{w_z}\left(\frac{\sqrt{2}r}{w_z}\right)^{|\ell|}L_p^{|\ell|}\left(\frac{2r^2}{w_z^2}\right)$$
$$\times \exp\left[-\frac{r^2}{w_z^2}+i\left(\frac{kr^2}{2R_z}+\ell\phi-(2p+|\ell|+1)\varphi_g\right)\right], \quad (1)$$
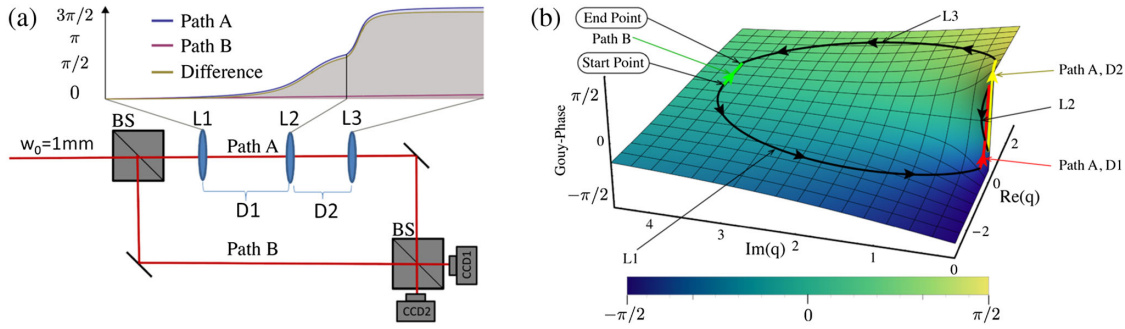
103601-1

FIG. 1. Accumulated Gouy phase interferometer. (a) Schematic of the theoretical setup with accumulated Gouy phase. A Mach-Zehnder interferometer with three lenses ($L1$, $L2$, $L3$: 500, 40, 300 mm; $D1$, $D2$: 560.8, 344.3 mm for a 1 mm collimated incoming beam) in one arm. The phase difference is introduced by propagating the beam through the three lenses. We obtain the accumulated Gouy phase difference $\Delta\varphi_g = (3\pi/2) = -(\pi/2)$. The device can sort light beams depending on the p and ℓ values, which will be detected through the two cameras CCD1 or CCD2. (b) Complex q-parameter space: The complex beam parameter q determines the spatial shape of a Gaussian beam—its beam waist and radius of curvature—unambiguously. The Gouy phase of a beam can be determined as a function of q, which is the plotted surface. The accumulated Gouy phase of a beam while propagating freely is given by the height difference on the surface. Here, the green line corresponds to free propagation in path B, while the red and yellow line corresponds to the propagation after $L1$ and after $L2$, respectively. The black lines indicate the action of the lenses in the q space: Both z and z_R change discretely, which gives a jump in the q space. The shape of the black curves is calculated from a continuous transition of the lens from $f = \infty$ to $f = 500$, $f = 40$, and $f = 300$ mm, respectively. In order to interfere, the two beams in path A and B must have the same spatial properties, i.e., must have the same q parameter. Thus, the end point of the green line must be at the end point of the black line for lens $L3$.

with the mode number ℓ denoting the orbital angular momentum (in units of $\hbar$) and p the radial mode number. $L_p^{|\ell|}$ are the Laguerre polynomials, $w_z = w_0\sqrt{1 + (z/z_R)^2}$ is the beam waist with w_0 being the beam waist at the focus. $z_R = (\pi w_0^2)/\lambda$ is the Rayleigh range, $R_z = z[1 + (z_R/z)^2]$ is the radius of curvature, λ is the wavelength, and $k = (2\pi)/\lambda$ is the wave number. $\varphi_g = \arctan(z/z_R)$ denotes the Gouy phase and is multiplied with the mode order $m = (2p + |\ell| + 1)$.

This phase is accumulated by Gaussian beams when they propagate through the focus, and was first observed by Louis Georges Gouy in 1890. Several physical interpretations have been given, such as the geometric effect of the Gaussian beam [32], as a geometric [33] or topological phase [34], or a phenomena arising due to an uncertainty relation [35]. The Gouy phase has been used with higher-order Gaussian modes, for example, to convert between higher-order modes [36] or to interferometrically sort Hermite-Gauss modes [37,38].

We use an interferometer, where one of the two arms contains a lens configuration and thus accumulates a different Gouy phase [39,40], as shown in Fig. 1(a). When they recombine, the two beams have the same spatial dimensions (beam waist and radius of curvature) but a mode-dependent phase difference $m \cdot \Delta\varphi_g$. If the phases are fractions of π, the interferometer can be used to sort higher-order Gaussian modes. The action of the interferometer can be intuitively understood in a geometric way, shown in Fig. 1(b). For that, we take advantage of the complex beam parameter $q = z + iz_R$, which completely determines the spatial properties of (higher order) Gaussian

beams after propagation through a lens system. Thus, also the Gouy phase can be written in terms of q as $\varphi_g(q) = \arctan[\text{Re}(q)/\text{Im}(q)]$, where Re() and Im() stand for the real and imaginary part of the complex q parameter. One can plot the Gouy phase in the complex q space, where the two coordinates are the real and imaginary part of the q parameter. In this space, one can plot the propagation of the two beams, and directly observe the accumulation of the Gouy phase, as shown in Fig. 1(b). The free-space propagation of a Gaussian beam continuously changes $\text{Re}(q)$, while a lens performs a discrete jump in the complex q space (as it discretely changes z and z_R at the same time).
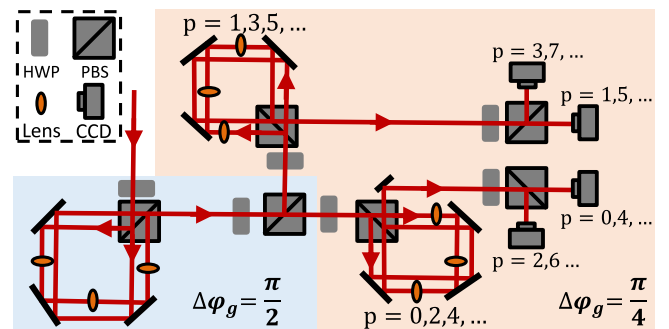

FIG. 2. To sort higher mode numbers, one could cascade the interferometers (a folded Sagnac-interferometer for long-term stability). Combining three such interferometers allows for sorting modes from $p = 0$ to $p = 3$: The first interferometer (with blue background) sorts even and odd modes, while the subsequent two interferometers sort $p = 0/p = 2$ and $p = 1/p = 3$, respectively. In our experiments, we show the results for both types of interferometers.
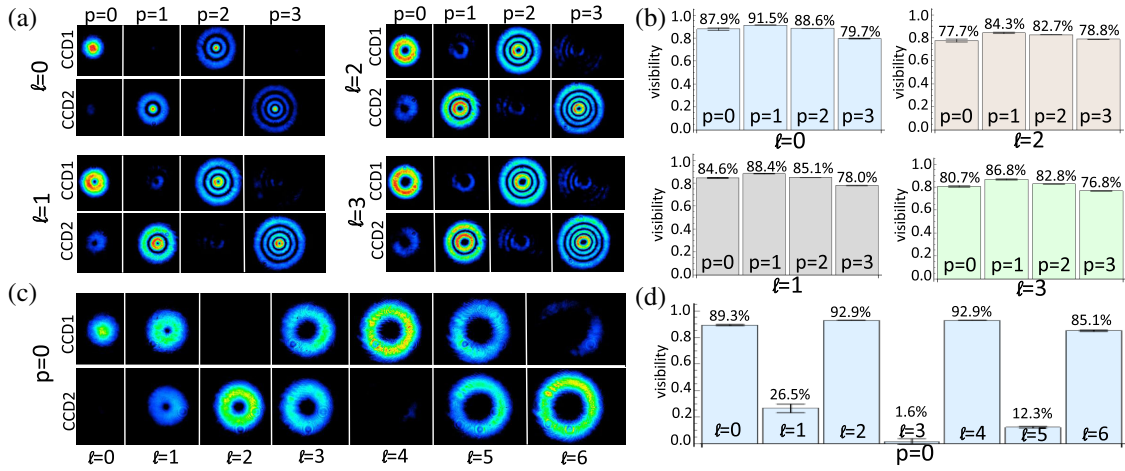
FIG. 3. Experimental results for p and ℓ modes in a $\Delta\varphi_g = (\pi/2)$ interferometer. (a) We show the sorting of four different p modes from $p = 0$ to $p = 3$, with different OAM values of $\ell = 0 - 3$. The intensity images taken with CCD cameras clearly show high quality sorting of different mode orders. To quantify the quality, we calculate the visibility $vis = |(P_1 - P_2)/(P_1 + P_2)|$ (where P_i stands for the power in the output arm i). All visibilities are beyond 75%. The errors stand for statistical uncertainties calculated from 10 independent measurements. (c)–(d) We measure OAM modes $\ell = 0$ to $\ell = 6$. Every even mode number is sorted, while every odd mode number is split and propagates to both detectors, which gives a vanishing visibility.

The Gouy phase difference is then the difference between the accumulated phase of the two beams.

By combining several of these interferometers, one can in principle access very high-dimensional mode spaces (see Fig. 2). Cascaded interferometers can be built extremely stable with modern production techniques (such as shown in Ref. [41], where 30 interferometers have been stable for more than 3 days with a visibility of more than 99%).

Experimental implementation.—We implement the experimental setup shown in Fig. 1(a) in order to sort higher-order Laguerre-Gauss modes, in particular their radial modes. For that, we require that the Gouy phase is a fraction of π, as well as that the resulting Gaussian beams have the same complex beam parameter q in order to interfere perfectly. With arbitrary, custom-tailored lens configurations, we could easily find such configurations [as it is indicated in Fig. 1(b)]. However, we restrict ourselves to standard lenses which are easily commercially available (see Supplemental Material [42] for a list of lenses). We use the computer algorithm MELVIN to search for suitable experimental configurations [31]. We found setups using three lenses in one of the arms, for $\Delta\varphi_g = (\pi/n)$ with $2 \le n \le 8$ in the Supplemental Material [42], and it is straightforward to find other phase configurations.

Experimentally we realized $\Delta\varphi_g = (\pi/2)$ and $\Delta\varphi_g = (\pi/4)$, where both configurations use the same lenses but different distances $D1$ and $D2$ between them.

To ensure interference even with slightly different optical path length introduced by the lenses in one arm, we use a $\lambda = 810$ nm laser with a sufficiently long coherence length. To create higher-order Laguerre-Gauss modes with a high quality, we use a phase-only spatial light modulator (SLM),

and apply the method to generate such modes suggested in Ref. [43].

Radial modes are dependent on the beam waist; thus, it is intuitively clear that the interferometer requires that the input beam has specific properties to give correct Gouy phases (in our case, $\lambda = 810$ nm, $w_0 = 1$ mm, $z = 0$ m). For long-term stability, we build the interferometer in a double-path Sagnac configuration (see Supplemental Material [42] for details on the experimental setup). After the interferometer, we split the output beams and direct them to two CCDs (which we use to image the output modes) and two power meters (which we use to measure the interference visibilities).

Experimental results for ($\pi/2$).—In order to produce $\Delta\varphi_g = (\pi/2)$, we use $L1 = 500$, $L2 = 40$, $L3 = 300$, $D1 = 560$, and $D2 = 343$ mm and a corresponding free-space
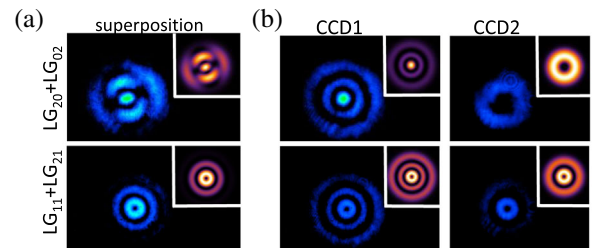

FIG. 4. Mode superpositions $\psi = (1/\sqrt{2})(LG_{2,0} + LG_{0,2})$ and $\psi = (1/\sqrt{2})(LG_{1,1} + LG_{2,1})$. (a) The images show the intensity of the superposition, the inset shows the theoretical intensity distribution. (b) Measured intensity distributions. The following two images show the output of the CCDs in the two output arms. As the modes have different mode numbers, they are sorted to different outputs of the interferometer.
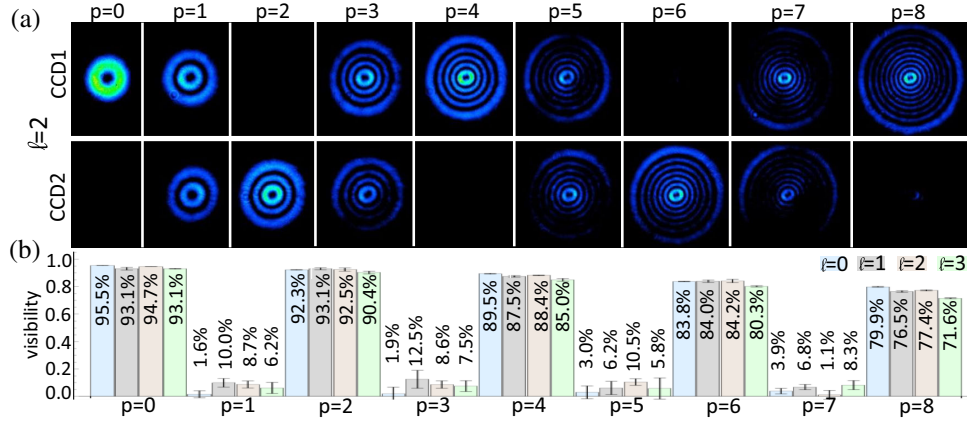
FIG. 5.   Experimental results for p and ℓ modes in a $\Delta\varphi_g = (\pi/4)$ interferometer. (a) Here we show an example for $\ell = 2$, $p = 0 - 8$. From the two CCD outputs, we clearly see that modes with even p constructively or destructively interfere, while modes with odd p split randomly. (b) The corresponding visibilities are consistently larger than 75%. Even modes with up to $p = 8$, $\ell = 2$ (which has a mode order of $m = (2p + \ell + 1) = 19$) can be interfered well beyond 75%. The errors stand for statistical uncertainties calculated from 10 independent measurements.

propagation length in path B of $D = D1 + D2 = 903$ mm. In Figs. 3(a) and 3(b), we show the results for sorting the radial p modes from $p = 0$ to $p = 3$ (with $\ell = 0, 1, 2$, and 3). The visibilities are all above 75%, and 83.5% on average. In Figs. 3(c) and 3(d), we show the sorting of ℓ modes, every even mode is sorted, while every odd mode is equally separated in both output ports. We measure $\ell = 0–6$ for $p = 0$ ($\ell = 0–6$ with $p = 1, 2$, and 3 can be seen in the Supplemental Material [42]). The sorting efficiency is very high, leading to visibilities beyond 85%. Intuitively, one would expect a lower visibility for higher order modes. Instead, here we observe the highest visibility for the $p = 1$ radial mode. This has two reasons: Deviations of the experimentally generated input beam q_{in} (beam waist w_0 and focus position z) from the ideal beam; and small errors in the distances between the three lenses. These misalignments lead to a slightly different accumulated Gouy phase difference, with the effect that higher order modes are sorted less efficient. Additionally, they also lead to different complex q parameters for the two paths A and B, and therefore to Newton rings which lower the interference visibility. None of the above two reasons are of fundamental nature and can be overcome with carefully designing and manufacturing the interferometric device.

In order to show that our proposed method is also capable for possible quantum applications, we investigate the device's capability of sorting coherent superpositions of different radial and OAM modes. In Fig. 4, we show the measurement results for coherent superpositions of LG modes with different orthogonal modes. In particular, we show the coherent superposition of $\psi = (1/\sqrt{2})(\text{LG}_{2,0} + \text{LG}_{0,2})$ and $\psi = (1/\sqrt{2})(\text{LG}_{1,1} + \text{LG}_{2,1})$. High quality separation of the superposition is clearly visible.

Experimental results for ($\pi/4$).—The device explained above can sort modes with even and odd p values. However, it cannot separate two even p values. With simple adjustments of the lenses ($D1 = 506$ and $D2 = 326$ mm), we are able to perform a $\Delta\varphi_g = (\pi/4)$ phase shift which can separate even and odd $p/2$ modes, such as $p = 0$ and $p = 2$—as shown in Fig. 5(a). In Fig. 5(b), the sorting visibilities of LG modes with $\ell = 2$ and $p = 0$ to $p = 8$ are shown. Every odd mode is equally separated, while the even modes are sorted. All visibilities are beyond 85% for $p \leq 4$ and larger than 75% for all modes smaller or equal to $\text{LG}_{p=8,\ell=2}$.

Conclusion.—We have identified and realized a method to interferometrically sort higher-order spatial Gaussian modes using accumulated Gouy phases. Particularly, it allowed us to experimentally sort radial Laguerre-Gaussian modes. It is also possible to cascade several p-mode sorters to increase the independently accessible modes, or to combine it with OAM-mode sorters [6] to access the complete set of spatial modes. This can readily be used for multiplexing and demultiplexing technologies in high-speed classical communication schemes. Our presented method can also be used in quantum optics as an in principle lossless two-input two-output device. This is in direct analogy to the polarizing beam splitter which is the workhorse for multiphoton qubit entanglement experiments [44]. The p-mode sorter expands the toolbox to manipulate higher-dimensional quantum states [10] and generate multiphoton high-dimensional entanglement [45,46]. It can also be used to create controlled quantum gates (e.g., CNOT gates) exploiting hybrid systems involving radial spatial modes. Having access to the radial modes would allow quantum teleporation of multiple degrees of freedom of a photon [47]. In particular, it could enable us to

teleport the complete quantum information encoded in the two-dimensional transverse plane of a single photon. Two basic building blocks for arbitrary high-dimensional unitary transformations are the generalized X and Z gate [11,48]. Our demonstrated p-mode sorter implicitly uses a generalized Z gate (the lens system). The high-dimensional X gate requires individual access to different parities (which we have demonstrated here) as well as a mode shifter. Thus the last missing experimental tool to generate arbitrary unitary transformations in the radial degree of freedom is the possibility to shift modes by a constant value. The implementation of such a mode shifter remains an important open question.

Note added.—Recently, we learned about a similar research project [49]. There, the authors solve the question for the p-mode dependent phase in a different way: They use a fractional Fourier transform for which the p modes are eigenfunctions.

---

[*]xmgu@smail.nju.edu.cn
[†]mario.krenn@univie.ac.at
[‡]anton.zeilinger@univie.ac.at

 [1] M. J. Padgett, Orbital angular momentum 25 years on, Opt. Express **25**, 11265 (2017).
 [2] L. Allen, M. W. Beijersbergen, R. Spreeuw, and J. Woerdman, Orbital angular momentum of light and the transformation of Laguerre-Gaussian laser modes, Phys. Rev. A **45**, 8185 (1992).
 [3] L. Marrucci, C. Manzo, and D. Paparo, Optical Spin-To-Orbital Angular Momentum Conversion in Inhomogeneous Anisotropic Media, Phys. Rev. Lett. **96**, 163905 (2006).
 [4] G. Campbell, B. Hage, B. Buchler, and P. K. Lam, Generation of high-order optical vortices using directly machined spiral phase mirrors, Appl. Opt. **51**, 873 (2012).
 [5] R. Fickler, G. Campbell, B. Buchler, P. K. Lam, and A. Zeilinger, Quantum entanglement of angular momentum states with quantum numbers up to 10,010, Proc. Natl. Acad. Sci. U.S.A. **113**, 13642 (2016).
 [6] J. Leach, M. J. Padgett, S. M. Barnett, S. Franke-Arnold, and J. Courtial, Measuring the Orbital Angular Momentum of a Single Photon, Phys. Rev. Lett. **88**, 257901 (2002).
 [7] G. C. Berkhout, M. P. Lavery, J. Courtial, M. W. Beijersbergen, and M. J. Padgett, Efficient Sorting of Orbital Angular Momentum States of Light, Phys. Rev. Lett. **105**, 153601 (2010).
 [8] M. P. Lavery, D. J. Robertson, G. C. Berkhout, G. D. Love, M. J. Padgett, and J. Courtial, Refractive elements for the measurement of the orbital angular momentum of a single photon, Opt. Express **20**, 2110 (2012).
 [9] M. Mirhosseini, M. Malik, Z. Shi, and R. W. Boyd, Efficient separation of the orbital angular momentum eigenstates of light, Nat. Commun. **4**, 2781 (2013).
[10] Y. Zhang, F. S. Roux, T. Konrad, M. Agnew, J. Leach, and A. Forbes, Engineering two-photon high-dimensional states through quantum interference, Sci. Adv. **2**, e1501165 (2016).
[11] A. Babazadeh, M. Erhard, F. Wang, M. Malik, R. Nouroozi, M. Krenn, and A. Zeilinger, High-Dimensional Single-Photon Quantum Gates: Concepts and Experiments, Phys. Rev. Lett. **119**, 180510 (2017).
[12] J. Wang, J. Y. Yang, I. M. Fazal, N. Ahmed, Y. Yan, H. Huang, Y. Ren, Y. Yue, S. Dolinar, M. Tur *et al.*, Terabit free-space data transmission employing orbital angular momentum multiplexing, Nat. Photonics **6**, 488 (2012).
[13] H. Huang, G. Xie, Y. Yan, N. Ahmed, Y. Ren, Y. Yue, D. Rogawski, M. J. Willner, B. I. Erkmen, K. M. Birnbaum *et al.*, 100 Tbit/s free-space data link enabled by three-dimensional multiplexing of orbital angular momentum, polarization, and wavelength, Opt. Lett. **39**, 197 (2014).
[14] M. Krenn, J. Handsteiner, M. Fink, R. Fickler, R. Ursin, M. Malik, and A. Zeilinger, Twisted light transmission over 143 km, Proc. Natl. Acad. Sci. U.S.A. **113**, 13648 (2016).
[15] M. P. Lavery, C. Peuntinger, K. Günthner, P. Banzer, D. Elser, R. W. Boyd, M. J. Padgett, C. Marquardt, and G. Leuchs, Free-space propagation of high-dimensional structured optical fields in an urban environment, Sci. Adv. **3**, e1700552 (2017).
[16] A. Mair, A. Vaziri, G. Weihs, and A. Zeilinger, Entanglement of the orbital angular momentum states of photons, Nature (London) **412**, 313 (2001).
[17] A. C. Dada, J. Leach, G. S. Buller, M. J. Padgett, and E. Andersson, Experimental high-dimensional two-photon entanglement and violations of generalized Bell inequalities, Nat. Phys. **7**, 677 (2011).
[18] J. Romero, D. Giovannini, S. Franke-Arnold, S. Barnett, and M. Padgett, Increasing the dimension in high-dimensional two-photon orbital angular momentum entanglement, Phys. Rev. A **86**, 012334 (2012).
[19] A. Vaziri, G. Weihs, and A. Zeilinger, Experimental Two-Photon, Three-Dimensional Entanglement for Quantum Communication, Phys. Rev. Lett. **89**, 240401 (2002).
[20] S. Gröblacher, T. Jennewein, A. Vaziri, G. Weihs, and A. Zeilinger, Experimental quantum cryptography with qutrits, New J. Phys. **8**, 75 (2006).
[21] M. Mirhosseini, O. S. Magaña-Loaiza, M. N. O'Sullivan, B. Rodenburg, M. Malik, M. P. Lavery, M. J. Padgett, D. J. Gauthier, and R. W. Boyd, High-dimensional quantum cryptography with twisted light, New J. Phys. **17**, 033033 (2015).
[22] A. Sit, F. Bouchard, R. Fickler, J. Gagnon-Bischoff, H. Larocque, K. Heshami, D. Elser, C. Peuntinger, K. Günthner, B. Heim *et al.*, High-dimensional intracity quantum cryptography with structured photons, Optica **4**, 1006 (2017).
[23] E. Karimi and E. Santamato, Radial coherent and intelligent states of paraxial wave equation, Opt. Lett. **37**, 2484 (2012).
[24] E. Karimi, R. Boyd, P. Hoz, H. Guise, J. Řeháček, Z. Hradil, A. Aiello, G. Leuchs, and L. L. Sánchez-Soto, Radial quantum number of Laguerre-Gauss modes, Phys. Rev. A **89**, 063813 (2014).

[25] W. N. Plick and M. Krenn, Physical meaning of the radial index of Laguerre-Gauss beams, Phys. Rev. A **92**, 063841 (2015).

[26] E. Karimi, D. Giovannini, E. Bolduc, N. Bent, F. M. Miatto, M. J. Padgett, and R. W. Boyd, Exploring the quantum nature of the radial degree of freedom of a photon via Hong-Ou-Mandel interference, Phys. Rev. A **89**, 013829 (2014).

[27] V. Salakhutdinov, E. Eliel, and W. Löffler, Full-Field Quantum Correlations of Spatially Entangled Photons, Phys. Rev. Lett. **108**, 173604 (2012).

[28] M. Krenn, M. Huber, R. Fickler, R. Lapkiewicz, S. Ramelow, and A. Zeilinger, Generation and confirmation of a (100×100)-dimensional entangled quantum system, Proc. Natl. Acad. Sci. U.S.A. **111**, 6243 (2014).

[29] R. Fickler, M. Ginoya, and R. W. Boyd, Custom-tailored spatial mode sorting by controlled random scattering, Phys. Rev. B **95**, 161108 (2017).

[30] R. Ionicioiu, Sorting quantum systems efficiently, Sci. Rep. **6**, 25356 (2016).

[31] M. Krenn, M. Malik, R. Fickler, R. Lapkiewicz, and A. Zeilinger, Automated Search for New Quantum Experiments, Phys. Rev. Lett. **116**, 090405 (2016).

[32] R. W. Boyd, Intuitive explanation of the phase anomaly of focused light beams, J. Opt. Sci. Am. **70**, 877 (1980).

[33] R. Simon and N. Mukunda, Bargmann Invariant and the Geometry of the Güoy Effect, Phys. Rev. Lett. **70**, 880 (1993).

[34] D. Subbarao, Topological phase in Gaussian beam optics, Opt. Lett. **20**, 2162 (1995).

[35] S. Feng and H. G. Winful, Physical origin of the Gouy phase shift, Opt. Lett. **26**, 485 (2001).

[36] M. W. Beijersbergen, L. Allen, H. Veen, and J. Woerdman, Astigmatic laser mode converters and transfer of orbital angular momentum, Opt. Commun. **96**, 123 (1993).

[37] J. Liñares, X. Prieto-Blanco, C. Montero-Orille, and V. Moreno, Spatial mode multiplexing/demultiplexing by Gouy phase interferometry, Opt. Lett. **42**, 93 (2017).

[38] J. Liñares, X. Prieto-Blanco, V. Moreno, C. Montero-Orille, D. Mouriz, M. C. Nistal, and D. Barral, Interferometric space-mode multiplexing based on binary phase plates and refractive phase shifters, Opt. Express **25**, 10925 (2017).

[39] M. F. Erden and H. M. Ozaktas, Accumulated Gouy phase shift in Gaussian beam propagation through first-order optical systems, J. Opt. Sci. Am. A **14**, 2190 (1997).

[40] K. Arai, LIGO Technical Note T1300189, 2013, https://dcc .ligo.org/LIGO-T1300189/public.

[41] X. L. Wang, Y. H. Luo, H. L. Huang, M. C. Chen, Z. E. Su, C. Liu, C. Chen, W. Li, J. X. Fang, J. Zhang, L. Li, N. L. Liu, C. Y. Lu, and J. W. Pan, 18-qubit entanglement with photon's three degrees of freedom, arXiv:1801.04043.

[42] See Supplemental Material at http://link.aps.org/ supplemental/10.1103/PhysRevLett.120.103601 for detailed experimental scheme; theoretical analysis of the visibilities; experimental result of sorting OAM modes with constant p mode using $\pi/2$ phase and for sorting p modes with constant OAM for $\pi/4$; list of lenses used in the automated search for the experimental setups; experimetal setups for different Gouy phase differences.

[43] E. Bolduc, N. Bent, E. Santamato, E. Karimi, and R. W. Boyd, Exact solution to simultaneous intensity and phase encryption with a single phase-only hologram, Opt. Lett. **38**, 3546 (2013).

[44] J. W. Pan, Z. B. Chen, C. Y. Lu, H. Weinfurter, A. Zeilinger, and M. Żukowski, Multiphoton entanglement and interferometry, Rev. Mod. Phys. **84**, 777 (2012).

[45] M. Malik, M. Erhard, M. Huber, M. Krenn, R. Fickler, and A. Zeilinger, Multi-photon entanglement in high dimensions, Nat. Photonics **10**, 248 (2016).

[46] M. Erhard, M. Malik, M. Krenn, and A. Zeilinger, Experimental GHZ entanglement beyond qubits, arXiv:1708.03881.

[47] X. L. Wang, X. D. Cai, Z. E. Su, M. C. Chen, D. Wu, L. Li, N. L. Liu, C. Y. Lu, and J. W. Pan, Quantum teleportation of multiple degrees of freedom of a single photon, Nature (London) **518**, 516 (2015).

[48] A. Asadian, P. Erker, M. Huber, and C. Klöckl, Heisenberg-Weyl Observables: Bloch vectors in phase space, Phys. Rev. A **94**, 010301 (2016).

[49] Y. Zhou, M. Mirhosseini, D. Fu, J. Zhao, S. M. H. Rafsanjani, A. E. Willner, and R. W. Boyd, Sorting Photons by Radial Quantum Number, Phys. Rev. Lett. **119**, 263602 (2017).